5800–5814 *Nucleic Acids Research, 2006, Vol. 34, No. 20* *Published online 19 October 2006*
doi:10.1093/nar/gkl751

Stability of the 'L12 stalk' in ribosomes from mesophilic and (hyper)thermophilic Archaea and Bacteria

D. Shcherbakov*, M. Dontsova[1], M. Tribus, M. Garber[1] and W. Piendl

Biocenter, Division of Medical Biochemistry, Innsbruck Medical University, Fritz-Pregl-Strasse 3, 6020, Innsbruck, Austria and [1]Institute of Protein Research, RAS, Institutskaya 4, 142290, Pushchino, Russia

Received August 6, 2006; Revised and Accepted September 23, 2006

ABSTRACT

The ribosomal stalk complex, consisting of one molecule of L10 and four or six molecules of L12, is attached to 23S rRNA via protein L10. This complex forms the so-called 'L12 stalk' on the 50S ribosomal subunit. Ribosomal protein L11 binds to the same region of 23S rRNA and is located at the base of the 'L12 stalk'. The 'L12 stalk' plays a key role in the interaction of the ribosome with translation factors. In this study stalk complexes from mesophilic and (hyper)thermophilic species of the archaeal genus *Methanococcus* and from the Archaeon *Sulfolobus solfataricus*, as well as from the Bacteria *Escherichia coli*, *Geobacillus stearothermophilus* and *Thermus thermophilus*, were overproduced in *E.coli* and purified under non-denaturing conditions. Using filter-binding assays the affinities of the archaeal and bacterial complexes to their specific 23S rRNA target site were analyzed at different pH, ionic strength and temperature. Affinities of both archaeal and bacterial complexes for 23S rRNA vary by more than two orders of magnitude, correlating very well with the growth temperatures of the organisms. A cooperative effect of binding to 23S rRNA of protein L11 and the L10/L12$_4$ complex from mesophilic and thermophilic Archaea was shown to be temperature-dependent.

INTRODUCTION

With a few bacterial exceptions (e.g. *Thermotoga*, *Aquifex* and *Thermus*), all organisms able to grow optimally at or above 75°C are classified within the Archaea. In order to cope with extreme temperature conditions, the intrinsic stability of all macromolecular cell components must be increased in thermophilic organisms. Extrinsic factors, such as ions or biogenic amines may serve as stabilizing ligands. To understand protein functions and stability at high temperatures, the proteins from hyperthermophiles are the focus of intense research (1–3). The structural features regulating the thermal stability of supermolecular cell structures like ribosomes are less well studied.

Though the crystal structure of the *Thermus thermophilus* 30S subunit and 70S ribosome have been determined (4), very little is known still about the structural features regulating the inherent thermal stability of ribosomes in thermophiles. The mechanisms involved in thermal stabilization of the ribosome have been investigated in some detail only for the thermophilic archaeon *Sulfolobus solfataricus*. In particular, it was shown that the individual ribosomal components (rRNAs and r-proteins) are less thermostable than the ribosome as a whole. More extensive interactions of r-proteins and rRNAs in thermophiles, compared to mesophilic microorganisms, seem to play an essential role (5–8). In thermophiles the rRNAs (and thus the whole ribosome) are stabilized by a higher G + C content of helical rRNA structures, and a striking correlation between G + C content of the RNA stems and the optimal growth temperature has been reported (9,10). Moreover, the unusually high base modification levels of 16S and 23S rRNA in thermophiles might contribute to the thermal stabilization of the ribosome as well (11). The importance of base modifications for the thermo-stabilization of tRNAs has been investigated in *Methanococcus* (12).

Primary rRNA-binding proteins from thermophiles exhibit a much higher affinity for their specific rRNA sites compared to their mesophilic counterparts, as has been shown for r-proteins L1 (13), S8 (14), S4 (15) and S7 (16). This strong RNA–protein interaction observed for the (hyper)thermophilic complexes might make an important contribution to the thermostability of the ribosome. Analysis of the 3D structure of *T.thermophilus* 30S subunit revealed some special features of r-proteins enhancing RNA–protein affinity, which probably play a role in the stability of the ribosome at high temperatures: e.g. the extra C-terminal helix of TthS17 increasing protein–RNA contacts and zinc-binding modules in TthS4 and TthS14 (17,18).

*To whom correspondence should be addressed. Tel: +43 512 9003 70334/70335; Fax: +43 512 9003 73110; Email: Dmitriy.Shcherbakov@i-med.ac.at

The archaeal genus *Methanococcus* comprises mesophilic (*Methanococcus maripaludis*, *Methanococcus vannielii*, *Methanococcus voltae*; optimal growth temperature 35°C), thermophilic (*Methanococcus thermolithotrophicus*—65°C) and hyperthermophilic (*Methanococcus jannaschii*, *Methanococcus igneus*—85–88°C) species; for a phylogenetic tree of the genus *Methanococcus* see (19). Although the optimal growth temperature of the mesophiles is about 50°C below that of the hyperthermophiles, their genomic G + C contents are nearly identical. The genus *Methanococcus* is an ideal model system not only to study mechanisms of thermal adaptation (1,20), but also to investigate the strategies by which RNA-binding proteins fine-tune the affinity for their RNA targets. It was shown earlier that r-proteins L1 and S8 from hyperthermophiles exhibit a 100-fold, and their homologues from thermophiles exhibit a 10-fold, higher affinity for rRNA than their mesophilic counterparts (13,14).

The L12 stalk is composed of two or three dimers of r-protein L12 (in Bacteria designated L7/L12; L7 is L12, which carries an acetylated N-terminal Ser residue in Bacteria only) and a single copy of r-protein L10 and is located in the large ribosomal subunits from Bacteria, Archaea and Eukarya (proteins P0 and P1/P2). L12 is the only ribosomal protein present in more than a single copy per ribosome. The 'L12 stalk' was considered to be a pentameric $L10/L12_4$ complex in all organisms, but latest studies showed that it is a heptameric $L10/L12_6$ complex (one molecule of L10 and three L12 dimers) in some thermophilic bacteria [e.g. *T.thermophilus* (21) and *Thermotoga maritima* (22)]. The stalk complex bound to 23S rRNA via L10 forms a mobile region ('L12 stalk') on the large ribosomal subunit, which is involved in the interaction of the ribosome with elongation factors (where its high conformational mobility is essential). Furthermore, this stalk plays an important role in the control of translational accuracy (23,24).

In Bacteria the genes of r-proteins L10 and L12 constitute their own operon (Figure 1A) and L10 as part of the stalk complex functions as a translational autoregulator of the operon binding to the own mRNA (25). However, in Archaea the genes encoding r-proteins L10 and L12 are in tandem as part of the L1 operon (Figure 1B) and L10 does not have a regulatory function (26).

The stalk complex can be easily extracted from the ribosome and it readily reassociates with ribosomal core particles that lack the complex. The complex can be easily reconstituted from isolated L10 and L12. In Bacteria the

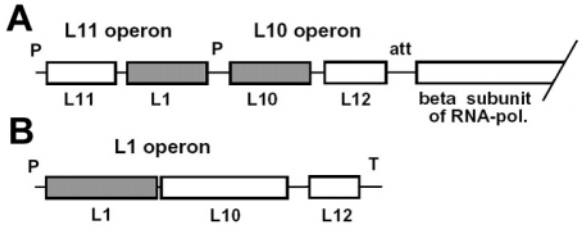

Figure 1. Transcriptional organization of the L10–L12 encoding region from (**A**) *E.coli* and (**B**) *Methanococcus spp*. Genes are shown as boxes. In the Bacterium *E.coli*, the L1 gene is part of another operon. The genes of the autoregulator proteins are shown in gray. P, promoter; T, terminator; att, attenuator.

L12 monomer includes two distinct structural domains linked by a flexible hinge (residues 37–52 in *Escherichia coli*); the elongated α-helical N-terminal domain (residues 1–36) is responsible for the dimer formation; the larger globular C-terminal domain (residues 53–120) probably interacts with elongation factors (27,28). Both L12 dimers are integrated into the ribosome through binding of their N-terminal domains to L10. L10 binds to a highly conserved target site in domain II of 23S rRNA [1029–1125 nt, *E.coli* nomenclature, (29)] close to the GTPase center of the 50S subunit. Intriguingly, archaeal L12 proteins and the eukaryal homologous P1/P2 proteins are shorter than their bacterial counterparts are, whereas L10 proteins from Archaea and P0 proteins from Eukarya have a C-terminal extension (about 80–100 amino acid residues), which does not exist in Bacteria (30). In Archaea and Eukarya, a high degree of sequence identity is apparent between the C-termini of the respective L10 and L12 proteins. The similarity of the archaeal and eukaryal stalk complexes is underlined by a recent study, which shows that hybrid ribosomes composed of *E.coli* 50S subunits and an archaeal stalk are accessible for archaeal as well as for eukaryotic elongation factors, but not for bacterial elongation factors (31).

The L12 stalk is missing on the electron density map of the 50S subunit (32,33) and of the 70S ribosome (4) probably due to its very high flexibility. However, the structure and properties of the isolated protein L12 from *E.coli* (EcoL12) have been studied in detail (34,35) as well as its conformational dynamic in the isolated form and within the ribosome (36,37). The crystal structures of the L12 monomer and dimer from *T.maritima* (TmaL12) have been determined (38). TmaL12 exists in two alternative monomer conformations that might reflect the suggested dynamic role of the protein in the translocation process. The mode of self-association of TmaL12 in solution has been studied in detail using a FRET study (39). Recently the crystal structure of bacterial TmaL10 in complex with three L12 N-terminal domain dimers was reported and the structure of the N-terminal domain of L10 from *Haloarcula marismortui* (HmaL10) on the 50S subunit was refined (22). Thus, the last major gap in the 3D structure of the ribosome could be filled.

Isolated L10 has a much lower rRNA-binding capacity than the $L10/L12_4$ complex, as shown for the L10 proteins from the mesophilic organisms *E.coli* (EcoL10) (37) and *M.vannielii* (MvaL10) (26). In this work, we demonstrated that this also holds true for L10 from the hyperthermophilic *M.jannaschii* (MjaL10).

In this study we characterized the interaction of a number of stalk complexes from mesophilic and (hyper)thermophilic Archaea (*Methanococcus* species and *S.solfataricus*) and from Bacteria (*E.coli*, *Geobacillus stearothermophilus* (formerly *Bacillus stearothermophilus*) and *T.thermophilus*) with their specific 23S rRNA target site at different temperatures, pH values and monovalent cation concentrations. We discovered a significant correlation of the affinity of $L10/L12_4$ complexes for 23S rRNA with the optimal growth temperature of the organisms. Both archaeal and bacterial stalk complexes from hyperthermophiles exhibit a much higher affinity for 23S rRNA compared to their mesophilic counterparts. Using a new two color fluorescence dye procedure for gel-shifts (40), we also examined a cooperative effect of

binding of the r-protein L11 and the $L10/L12_4$ complex to 23S rRNA. It was shown that this effect for mesophilic and thermophilic proteins is temperature-dependent and correlates with the optimal growth temperature of the organisms.

MATERIALS AND METHODS

Plasmid constructions

To construct the expression plasmids listed in Table 1 genomic DNA, prepared as described in (41), was used as a template to amplify the genes encoding the r-proteins by PCR, using either an Advantage® 2 PCR Kit (CLONTECH) or a ProofStart™ PCR Kit (QIAGEN), both of which provide an antibody-mediated 'hot start' and proofreading activity. The sequences of the relevant genes, available in the PubMed GeneBank or PEDANT genome databases, were used to design the PCR primers (synthesized by Microsynth, Switzerland). To express the r-proteins in *E.coli* the genes were cloned into the high-level expression vector pET11c (42). For this purpose, two restriction sites were created by PCR upstream and downstream of the coding sequences. The primer at the 5′ end of the gene had an NdeI site (including the ATG start codon); the primer at the 3′ end had a BamHI site downstream of the stop codon. The annealing temperatures for each PCR were optimized individually in the range of 50 to 64°C. NdeI–BamHI fragments carrying the genes of r-proteins were inserted in the corresponding sites of pET11c to generate expression plasmids (Table 1). To overproduce the stalk complexes in *E.coli*, the genes encoding L10 and L12 were cloned in pET11c as the original tandem present in the genome (Figure 1) and thus co-expressed; therefore the complexes were formed *in vivo* in the *E.coli* cells and purified in the intact state.

Three DNA fragments encoding the complete 23S rRNA-binding sites for $L10/L12_4$ complexes from *M.jannaschii*, *M.thermolithotrophicus* and *S.solfataricus* were amplified by PCR and cloned into vector pUC18. Each PCR fragment contained the T7 promoter and sites for the restriction enzymes BamHI (upstream) and SmaI (downstream) for cloning; the SmaI site was used also for linearization of the plasmid before transcription. The correct sequences of the cloned PCR products were confirmed by double-stranded sequencing (Microsynth, Switzerland).

Synthesis of the 23S rRNA fragments

23S rRNA fragments were transcribed *in vitro* using T7 RNA polymerase (Fermentas) from linearized plasmids or DNA fragments amplified by PCR. The DNA fragments amplified by PCR were synthesized using genomic DNA as a template; the upstream primer contains the T7 promoter sequence. To obtain the 23S rRNA fragments shorter than 95 nt containing deletions (see Table 2 and Figure 6) template DNA fragments were amplified by PCR using oligonucleotides as a template. The plasmids and DNA fragments used as templates for synthesis of the 23S rRNA fragments by T7 transcription are listed in Table 2.

^{32}P-labeled RNA fragments were prepared using the MAXIscript™ T7 *in vitro* Transcription kit (Ambion Inc.) in the presence of [α-^{32}P]UTP (800 Ci/mmol; New England Nuclear Corp.). Transcripts were purified using mini Quick Spin RNA Columns (Roche). To obtain the RNA in preparative scale the following procedure was used. A total of 1–3 ml of transcription mixture containing 80 mM HEPES/KOH (pH 7.5), 32 mM $MgCl_2$, 40 mM DTT, 4 mM each of NTPs, 0.2 mM spermidin, 200–300 μg/ml of linearized plasmid and 400–600 U/ml of T7 RNA polymerase was incubated at 37°C for 2–4 h. Next, unincorporated nucleotides and template DNA were removed by size exclusion chromatography on a K9/60 column packed with Superdex™ G-75 (Amersham Bioscience) in a buffer containing 50 mM sodium acetate (pH 5.5) and 5 mM $MgCl_2$. Fractions containing RNA were pooled and precipitated by ethanol. The purity and integrity of the RNA transcripts were verified by electrophoresis on 8% PAG containing 7 M urea.

Table 1. Plasmid constructs used to produce r-proteins and L10/L12 stalk complexes

Source organism	Name of construct	Products of expression
M.jannaschii	pMjaL10–12.4	MjaL10/$L12_4$; MjaL10
	pMjaL12.4	MjaL12
	pMjaL11.4	MjaL11
M.igneus	pMigL10–12.4	MigL10/$L12_4$
	pMigL12.4	MigL12
M.thermolithotrophicus	pMthL10–12.4	MthL10/$L12_4$
	pMthL12.4	MthL12
M.vannielii	pMvaL1.55M5 (60)	MvaL1; MvaL10/$L12_4$
S.solfataricus	pSsoL10–12.4	SsoL10/$L12_4$
T.thermophilus	pTthL10–12.4	TthL10/$L12_6$
G.stearothermophilus	pGstL10–12.4	GstL10/$L12_4$
E.coli	pEcoL10–12.4	EcoL10/$L12_4$

Overproduction and purification of the stalk complexes and of individual L10, L11 and L12 proteins

R-proteins and stalk complexes used in this study were isolated from *E.coli* BL21(DE3) (43) transformed with the respective plasmids. To obtain maximal yields of the recombinant proteins and to avoid a potential misincorporation of lysine instead of arginine as a result of the difference in codon usage between *Methanococcus* or *Sulfolobus* and *E.coli* (44), the archaeal r-proteins were overproduced in *E.coli* BL21(DE3) cells cotransformed with pUBS520, a plasmid that carries the genes for the rare $tRNAs^{Arg}_{AGA/AGG}$ (45). Usually, good yields of the recombinant proteins (up to 15–20% of total cellular protein) were obtained. The only exceptions were MjaL12 and MigL12 which, when overproduced in the absence of L10, gave rather low yields (<1% of total cellular protein).

As the purification protocol for MvaL10/$L12_4$ from *E.coli* cells described in (26) used partially denaturing conditions (a buffer with 4 M urea was used), we elaborated a new protocol (see below), which allows purification of the r-proteins and stalk complexes under non-denaturing conditions. Overproduction of recombinant proteins was induced by adding isopropyl-β-D-thiogalactopyranoside (IPTG) up to 0.1 mM after the density of the host cell culture reached an A_{600} of 0.6–0.8. 3–4 h after induction the *E.coli* cells were harvested by centrifugation and resuspended in 6–8 ml/g (wet mass) of a buffer containing 100 mM Tris–HCl (pH 8.0), 100 mM $MgCl_2$, 1 M NaCl, 1 mM DTT and 0.1 mM

Table 2. 23S rRNA fragments used for filter-binding assays and gel-shift experiments

Source organism	Name	Template used for transcription	Size of transcript, nt	Short description
M.jannaschii	pMja23S-95	Plasmid	95	Full-length binding site (boxed green in Figure 6B)
	Mja23S-80	PCR fragment	80	Binding site where helix 43a was deleted
	Mja23S-70	— // —	70	Binding site where whole helix 43 was deleted
	Mja23S-81	— // —	81	Binding site where helix 44 was deleted
	Mja23S-56	— // —	56	Binding site where both of helixes 43 and 44 were deleted
M.thermolithotrophicus	pMth23S-95	Plasmid	95	Full-length binding site (designed as Mja23S-95)
M.vannielii	pMvL10.23S	— // —	230	Complete L10 binding site in 23S rRNA from *M.vannielii* (26)
S.solfataricus	pSso23S-95	— // —	95	Full-length binding site (designed as Mja23S-95)
T.thermophilus	Tth23S-95	PCR fragment	95	— // —
G.stearothermophilus	Gst23S-95	— // —	95	— // —
E.coli	Eco23S-95	— // —	95	— // —

phenylmethlysulfonyl fluoride (PMSF). The resuspension buffer for MigL12, MjaL12 and MthL12 contained 100 mM Tris–HCl (pH 7.5), 100 mM LiCl, 1 M NaCl, 2 mM EDTA and 0.1 mM PMSF; that for EcoL10/$L12_4$ contained 100 mM Tris–HCl (pH 8.0), 50 mM $MgCl_2$, 150 mM NaCl, 70 mM NH_4Cl, 1 mM DTT and 0.1 mM PMSF. Cells were passed twice through a chilled French pressure cell at 10 000 psi; *E.coli* cell debris and ribosomes were removed by two consecutive centrifugation steps (30 000 *g* for 30 min and 150 000 *g* for 2 h). In the case of MvaL10/$L12_4$ (see Table 1) co-expressed MvaL1 forming inclusion bodies was also removed by these centrifugation steps (26).

Further purification of the r-proteins and stalk complexes (with the exception of EcoL10/$L12_4$) was performed with heat treatment of the post-ribosomal fraction. The main contaminating proteins from *E.coli* host cells were denatured by heating for 20 min at 75°C (MjaL10/$L12_4$, MjaL11, MigL10/$L12_4$, MigL12, MjaL12 and TthL10/$L12_6$), 70°C (SsoL10/$L12_4$), 65°C (MthL10/$L12_4$, MthL12 and GstL10/$L12_4$) or 55°C (MvaL10/$L12_4$) and removed by centrifugation (30 000 *g* for 30 min). Surprisingly, MvaL10/$L12_4$ from the mesophilic *M.vannielii* is thermostable up to 60°C and thus the heat step could be included in the purification procedure. Next, the proteins were precipitated by adding $(NH_4)_2SO_4$ up to 0.6 g/ml and the resulting pellet, harvested by centrifugation (30 000 *g* for 30 min) was dissolved in a buffer containing 75 mM Na-acetate (pH 5.0), 50 mM NaCl, 1 mM DTT and loaded on a 5 ml cation-exchange chromatography HiTrap SP-Sepharose (Amersham Bioscience) column equilibrated with the same buffer. After washing with loading buffer the proteins were eluted with 40 ml of a linear gradient of 0–1 M NaCl and 1 ml fractions were collected. Fractions containing the stalk complex were pooled and dialyzed against a buffer containing 50 mM Tris–HCl (pH 8.0), 60 mM NH_4Cl, 25 mM NaCl, 1 mM DTT and loaded on a 5 ml anion-exchange chromatography HiTrap Q-Sepharose (Amersham Bioscience) column equilibrated with the same buffer. After washing with loading buffer the proteins were eluted with 40 ml of a linear gradient of 0–0.5 M NaCl. Fractions containing pure r-proteins or stalk complexes were pooled and concentrated using Vivaspin concentrators (Vivascience) or precipitated with $(NH_4)_2SO_4$ for storage. In the case of the MjaL10/$L12_4$ complex, L10, which was produced in excess over L12, was removed at the anion-exchange chromatography step. As for the purification of EcoL10/$L12_4$, only the extraction of this complex from native ribosomes was described (46). The purification procedure for recombinant EcoL10/$L12_4$ was in general the same as for the other complexes (see above), with a modified buffer for cation-exchange chromatography [50 mM sodium citrate (pH 4.0), 40 mM $(NH_4)_2SO_4$, 25 mM NaCl and 1 mM DTT].

After the anion-exchange chromatography purification step, MvaL10/$L12_4$ and EcoL10/$L12_4$ contained traces of RNase activity, which were removed by hydrophobic chromatography. Complexes, dissolved in a buffer containing 50 mM Tris–HCl (pH 8.0), 100 mM NaCl, 1.5 M $(NH_4)_2SO_4$ and 1 mM DTT, were loaded on a 5 ml hydrophobic chromatography HiTrap Butyl-Sepharose column (Amersham Bioscience) equilibrated with the same buffer and eluted with a 40 ml linear reverse gradient of 1.5–0 M $(NH_4)_2SO_4$. The purification procedure for L12 proteins included two consecutive anion-exchange chromatography steps on 5 ml HiTrap Q-Sepharose and HiTrap DEAE-Sepharose columns as described above. In both cases, the loading buffer contained 50 mM Tris–HCl (pH 7.5) and 50 mM LiCl. 40 ml linear gradients of 0–1 M NaCl (for Q-Sepharose) and 0–0.5 M $(NH_4)_2SO_4$ (for DEAE-Sepharose) were used to elute the proteins. The purity and homogeneity of the r-proteins and complexes were verified by SDS–PAGE, and gel filtration chromatography. Analytical gel filtration chromatography was performed on a Series 1050 high-performance liquid chromatography (HPLC) system (Hewlett-Packard) with a Superdex™-75 10/30 size exclusion column (Amersham Bioscience) in a buffer containing 50 mM Tris–HCl (pH 7.6), 7 mM $MgCl_2$, 30 mM KCl, 70 mM NH_4Cl and 1 mM DTT.

Protein analyses

The stoichiometry of the L10–L12 complexes was determined after the purification procedure as well as in an RNA-bound state ('active' state). Purified complexes were analyzed by SDS–PAGE, stained with fluorescent SYPRO® Tangerine Protein Gel Stain (Molecular Probes) and scanned using the TYPHOON 9410 Imaging System. The fluorescence intensity of each band was quantified and the amount of protein calculated using ImageQuant 5.2 software (Molecular Dynamics). To determine the stoichiometry of the L10–L12 complexes bound to RNA ('active' state) we used the method described in (47) with some modifications. Briefly, the purified stalk complex or a mixture of isolated L10 and L12 proteins in different molar ratios (1:2; 1:4;

1:6) were mixed with a 1.5 times molar excess of the 95 nt 23S rRNA fragment (Table 2) and loaded on a native 8% PAG. After electrophoresis the gel was stained with SYBR® Green I, bands corresponding to RNA–protein complexes were cut out and the slices were placed on a 15% SDS–PAG. During electrophoresis, each complex was resolved into two protein bands, corresponding to L10 and to L12. The PAG was stained with fluorescent SYPRO® Tangerine Protein Gel Stain, scanned and the fluorescence intensity of each band was quantified as described above.

In order to completely denature the tertiary (or quaternary, i.e. dimeric) structure of L12 proteins, which are probably not completely denatured in normal SDS–PAGE, the proteins were analyzed by electrophoresis in 20% PAG in the presence of SDS and 8 M urea. The loading buffer contained 80% formamide and 1% SDS. Samples were preheated for 10 min at 100°C. Gel electrophoresis and staining by Coomassie blue were performed according to standard techniques.

Samples of MigL12 and MthL12 proteins were analyzed by electrospray ion-mass-spectrometry (48) using a MAT 900 instrument (Finnigan/MAT GmbH). Samples (5–10 μg) were dissolved in 50% aqueous methanol containing 0.1% formic acid and injected into the ion source. The experiments were performed by H. Lindner, Biocenter, Innsbruck Medical University.

Analyses of RNA–protein complexes

Filter-binding assays. The affinities of L10 and L11 proteins and of the stalk complexes to their binding site on 23S rRNA were measured by a nitrocellulose filter-binding assay as described in (49). TMK_{350} binding buffer contained 50 mM Tris–HCl (pH 7.6), 20 mM $MgCl_2$, 350 mM KCl, 5 mM β-mercaptoethanol, 0.04% BSA. To test the influence of monovalent cations on RNA-binding, the KCl concentration varied in the range of 50 mM to 800 mM. Each binding curve was calculated from at least three independent experiments by non-linear regression using the computer package 'SPSS for Windows' Release 11.5 (SPSS Inc.). To determine the percentage of 'active' protein complexes (i.e. stalk complexes binding RNA) in our preparations, RNA excess assays were used. The assays were performed under standard conditions (TMK_{350} buffer, 37°C) as described above and contained 1 nM of archaeal $L10/L12_4$ and ^{32}P-labeled RNA in the range of 10 pM to100 nM in TMK_{350}.

PAGE under non-denaturing conditions. Protein, protein–protein and RNA–protein complexes were analyzed by electrophoresis using the Mini-PROTEAN II system (Bio-Rad) in a 6% PAG under non-denaturing conditions in a buffer containing 25 mM Tris–Boric acid (pH 7.5) and 5 mM $MgCl_2$. Samples were run for 2–4 h at 100 V at 4°C. After electrophoresis the protein components were stained with fluorescent SYPRO® Red Protein Gel Stain (Molecular Probes) and the RNA components were stained with SYBR® Green I (Roche). Alternatively, proteins were stained with fluorescent TAMRA (tetramethylrhodamine) before complex formation and gel electrophoresis. Stained gels were scanned using the TYPHOON 9410 Imaging System (Amersham Bioscience).

The gel retardation assays (gel-shifts) of the protein–protein and RNA–protein complexes are described in detail in (40). For the gel-shifts the samples were pre-incubated in binding buffer containing 50 mM Tris–HCl (pH 7.6), 7 mM $MgCl_2$, 30 mM KCl, 70 mM NH_4Cl and 1 mM DTT at 37°C (or 70°C) for 10 min before loading.

RESULTS

Characterization of the recombinant stalk complexes

Stalk complexes assembled in *E.coli* and purified under non-denaturing conditions were very stable and no dissociation during purification or storage was observed. All complexes, except that from *T.thermophilus* and *M.jannaschii*, seem to be formed in the host cells in a stoichiometry close to 1:4 (L10:L12), as estimated by scanning of SDS–PAGE gels stained with fluorescent SYPRO® Tangerine. The recombinant complex from *T.thermophilus* showed a ratio of 1:6 (L10:L12), and thus presumably the same heptameric structure (one molecule of L10 and three L12 dimers) was formed as previously described for complexes isolated from *Thermus* ribosomes (21). Only the MjaL10/L12 recombinant proteins were not produced in the ratio 1:4; therefore, there were less than 4 molecules of MjaL12 per molecule of MjaL10 in the host cells. MjaL12 was completely incorporated in pentameric $L10/L12_4$ complexes. Only free MjaL10, but no other potential intermediates like $L10/L12_2$, was detected. This observation is in agreement with a previous analysis of recombinant $EcoL10/L12_4$ which demonstrated that only $L10/L12_4$, but no other potential complexes (e.g. $L10/L12_2$), was formed (50).

The homogeneity as well as approximate MWs and linear dimensions of the stalk complexes in solution were tested by analytical gel filtration chromatography (data not shown). The analyses showed that L10 and L12 in solution form pentameric $L10/L12_4$ and heptameric $L10/L12_6$ (*T.thermophilus)* complexes, respectively. PAGE under non-denaturing conditions of $MjaL10/L12_4$, $MthL10/L12_4$ and $MvaL10/L12_4$ (Figure 2) revealed one or more additional high MW bands, which probably can be interpreted as dimeric and multimeric forms of the stalk complexes. Gel shift experiments revealed that the observed dimeric form of $MjaL10/L12_4$ binds RNA (Figure 2, lanes 2–4) whereas $MthL10/L12_4$ dimers (Figure 2, lanes 5–7) and the multimeric forms of MvaL10/L12 (Figure 2, lanes 8–10) have no affinity for the specific rRNA target site.

We also determined the stoichiometry of 'active' stalk complexes bound to their specific 23S rRNA-binding site. The protein–RNA complexes were visualized in non-denaturing PAGE by an RNA-specific dye, cut out and reanalyzed by SDS–PAGE with subsequent scanning and quantification of resulting bands (Figure 3). All 'active' protein complexes showed a molar ratio very close to 1:4 (L10:L12) and for $TthL10/L12_6$ a molar ratio of 1:6 (L10:L12) was observed (standard deviations were not more then 10%). Therefore, binding to their specific RNA target site does not influence the stoichiometry of the stalk complexes.

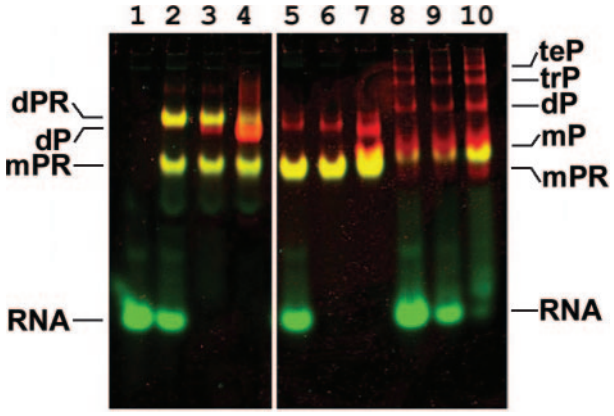

Figure 2. Interaction of archaeal L10/L12$_4$ complexes with the specific Mja23S-95 rRNA fragment analyzed by non-denaturing PAGE with two color fluorescent staining. The protein component is visualized with SYPRO® Red Protein Gel Stain (red) and the RNA component with SYBR® Green I (green). The yellow color represents the protein–RNA complexes because of the superimposed green and red signals from the RNA (SYBR Green I) and protein (SYPRO Red) channel. Lane 1, RNA fragment Mja23S-95; lanes 2–4, MigL10/L12$_4$ mixed with Mja23S-95 in a molar ratio of 1:2, 1:1, 2:1 respectively; lanes 5–7, MthL10/L12$_4$ mixed with Mja23S-95 in the same ratios; 8, 9, 10—MvaL10/L12$_4$ mixed with Mja23S-95 in a molar ratio of 1:4, 1:1, 4:1, respectively. R, RNA fragment Mja23S-95; mP(R), monomeric form of the L10/L12$_4$ (bound to RNA); dP(R),dimeric form of the L10/L12$_4$ (bound to RNA); trP,trimeric form of the L10/L12$_4$; teP, tetrameric form of the L10/L12$_4$.

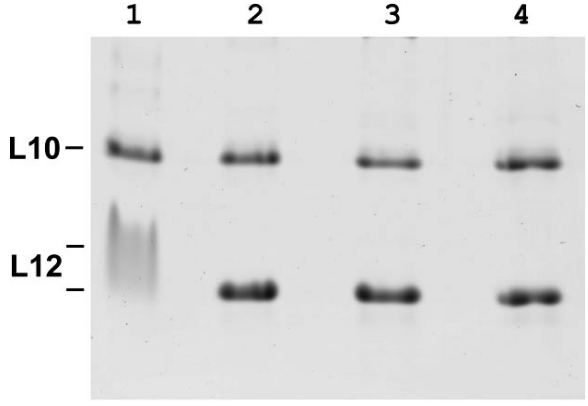

Figure 3. Analysis of stoichiometry of archaeal stalk complexes bound to the specific Mja23S-95 rRNA fragment. SDS–PAG was stained with SYPRO® Tangerine Protein Gel Stain for subsequent scanning and quantification. Lane 1, MigL10/L12$_4$; lane 2, MthL10/L12$_4$; lanes 3 and 4 MthL10, and MthL12 premixed in a molar ratio of 1:2 and 1:6, respectively.

Purified stalk complexes were tested by SDS–PAGE (Figure 4). Whereas the L10 proteins demonstrated mobility according to their MW, most of the archaeal L12 proteins had anomalous mobility. MvaL12 had an apparent MW of about 10 000 (Figure 4, lane 7), which is in agreement with the calculated MW of 9819. MthL12, which has almost the same calculated MW and pI as MvaL12 (10 294 and 4.34 in comparison with 9819 and 4.56), formed a clear-cut band on SDS–PAGE corresponding to a MW of about 14 000–15 000 as isolated protein (Figure 3, lane 9), as well as part of the MthL10/L12$_4$ complex (Figure 4, lane 6). Protein SsoL12 had an apparent MW of about 17 000 on SDS–PAGE (Figure 4, lane 10) which is much higher than the calculated MW of 11 292. MjaL12 and MigL12, with MWs and pIs almost identical to those of MthL12, formed diffuse bands on the gel in the range of approximately 14 000 to 24 000 (Figure 4, lanes 4 and 5).

To exclude incomplete denaturation of very stable L12 dimers (or of the tertiary structure of L12 monomers), the denaturing effect of SDS was increased by adding urea (8 M) to the SDS–PAG and formamide (90%) to the loading buffer. The increase of the denaturing effect by urea did not notably affect the mobility of most of the archaeal L12 proteins (Figure 5). Only SsoL12 and MvaL12 migrated according to their calculated MWs; MigL12 and MjaL12 formed clear-cut bands (in contrast to diffused bands on standard SDS–PAG) with apparent MWs of 20 000 and 17 000, respectively, which is approximately twice as high as the calculated MWs.

To prove that the *E.coli* host synthesized correct recombinant L12 proteins, the exact MWs of MigL12 and MthL12 were analyzed by mass-spectrometry as described in Materials and Methods. Mass spectra of MigL12 showed two major peaks at 10 290.0 and 10 319.0 (calculated MW 10 291). Mass spectra of MthL12 also had two major peaks at 10 292.0 and 10 319.0 (calculated MW 10 293). The additional peak can be explained by the presence of bound inorganic ion(s) (e.g. Mg^{++}). Thus, the mass spectra documented that both recombinant proteins, MigL12 and MthL12, are of the correct size and contain no post-translational modifications.

Design of a 'minimal' 23S rRNA fragment carrying the L10 binding site

The binding site of the stalk complex is located in domain II of 23S rRNA and includes three helices (H42, H43 and H44) and several loops (Figure 6A) (51). Early chemical protection, hydroxyl radical and enzymatic probing experiments established that L11 (and thiostrepton) interact with the apical hairpin and basal impaired nucleotides of helix 43 (Figure 6A), whereas the L10 binding site includes helix 42 almost completely (51,52). These data were confirmed by the crystal structure of the L11–rRNA complex (53,54) and the refinement of a L10$_{NTD}$–23S rRNA complex (22).

In this work we constructed a 'minimal' 23S rRNA fragment—an RNA fragment as short as possible which still would retain the full affinity for the stalk complex. Four fragments of *M.jannaschii* 23S rRNA, in which either helix 43a (Figure 6B, box I), helix 43 (Figure 6B, box II), helix 44 (Figure 6B, box III) or both helixes 43 and 44 (Figure 6B, boxes II and III) were deleted, were analyzed for their L10/L12$_4$ binding capacity using filter-binding experiments. A 230 nt fragment of 23S rRNA from *M.vannielii* carrying the L10 binding site (1063–1292 nt, *M.vannielii* nomenclature) (26) was used as a control. Typical binding curves for the interaction of MjaL10/L12$_4$ with the RNA fragments are presented in Figure 7. Deletions of helixes 43 and/or 44 led to a complete loss of the affinity for the stalk complex. The deletion of helix 43a slightly reduced the affinity for L10/L12$_4$ (average dissociation constant, K_d of $9 \pm 3 \times 10^{-10}$ M for Mja23S-95 and K_d of

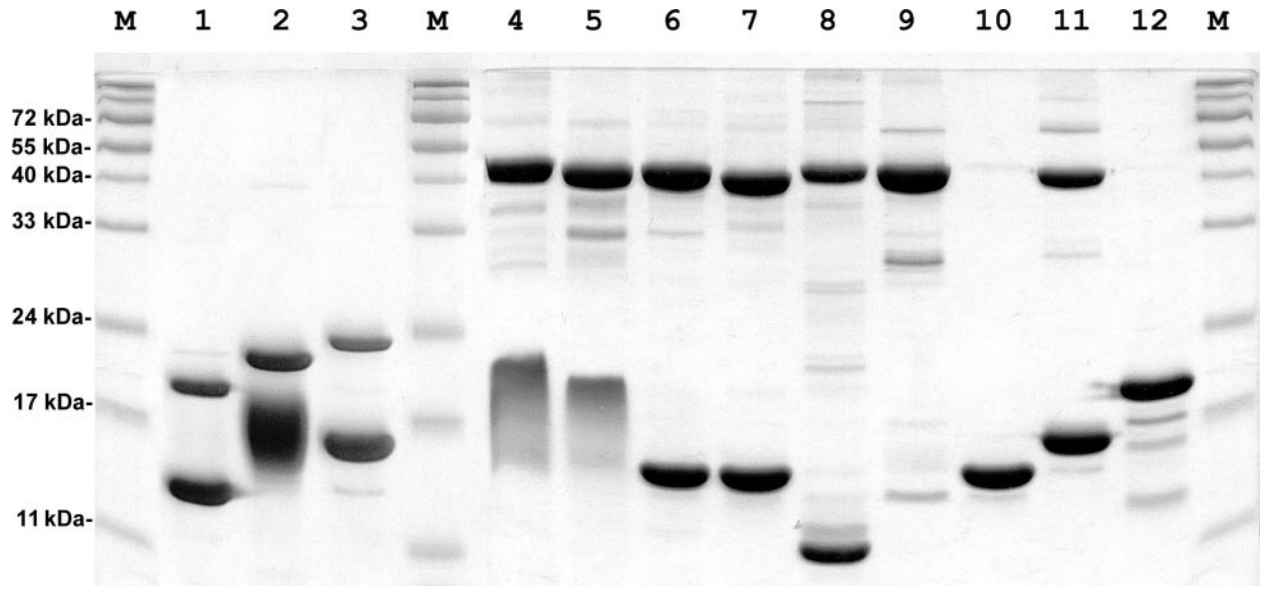

Figure 4. Archaeal and bacterial stalk complexes and individual r-proteins L10, L11 and L12 analyzed by SDS–PAGE (18%). M, Protein size marker; 1, TthL10/$L12_6$; 2, GstL10/12_4; 3, EcoL10/$L12_4$; 4, MigL10/$L12_4$; 5, MjaL10/$L12_4$; 6, MthL10/$L12_4$; 7, MvaL10/$L12_4$; 8, MjaL10; 9, MthL12; 10, SsoL10/$L12_4$; 11, MjaL11.

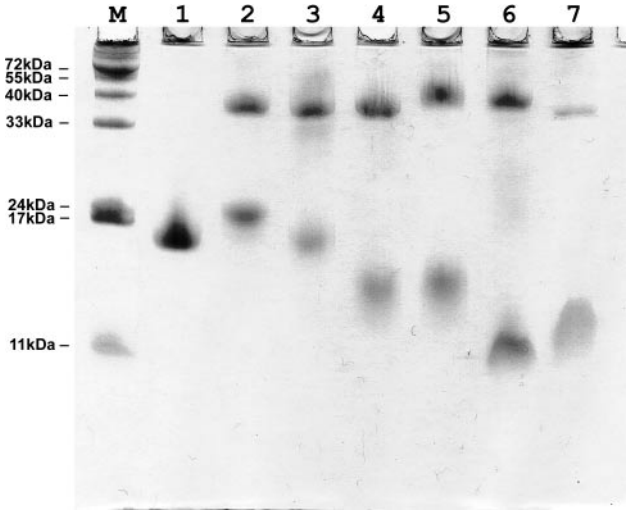

Figure 5. Archaeal L10/$L12_4$ complexes analyzed by SDS–PAGE (15%) in the presence of 8 M urea. MjaL11 is used for comparison. M, Protein size marker; 1, MjaL11; 2, MigL10/$L12_4$; 3, MjaL10/$L12_4$; 4, MthL10/$L12_4$; 5, MvaL10/$L12_4$; 6, SsoL10/$L12_4$.

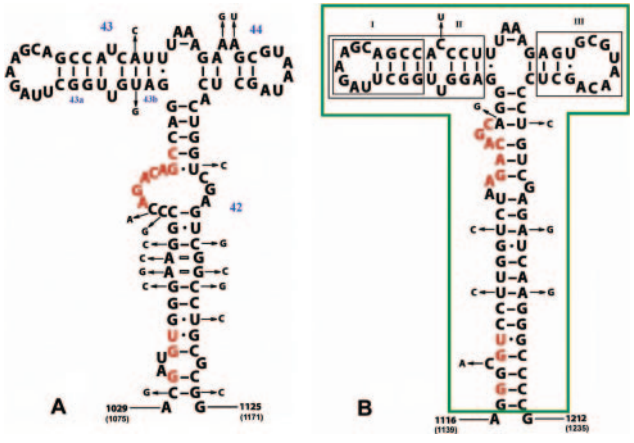

Figure 6. Secondary structures of the bacterial (**A**) and archaeal (**B**) L10 binding sites on 23S rRNA. (A): RNA fragment from *E.coli*, nucleotide changes in *T.thermophilus* are indicated; numbering of the helixes is according to (29) and marked in blue; (B): RNA fragment from *M.vannielii*, nucleotide changes in *M.jannaschii* are indicated. The conserved core in helix 42, thought to be the essential element for binding of the stalk complex (51,52), is marked in red. The parts of the archaeal RNA fragment, which were deleted (I; II; III; II and III) are boxed in black. The 95 nt fragment, which was finally used for binding experiments is boxed in green.

$3 \pm 0.4 \times 10^{-9}$ M for Mja23S-80), but the saturation level of binding decreased from 75 to 35%. The 95 nt RNA fragment (boxed green in the Figure 6B) retained the full affinity for the stalk complex. Therefore, Mja23S-95 was used in all binding experiments. In addition, 95 nt 23S rRNA fragments from different Archaea and Bacteria (listed in Table 2) were used to test the affinity of stalk complexes for their homologous rRNA target site. As this part of 23S rRNA is extremely conserved among Bacteria and Archaea (Figure 6A and B), the 95 nt fragments were designed according to the 'minimal' Mja23S-95 fragment. These fragments might also be suitable for future crystallization experiments of L10/$L12_4$–23S rRNA complexes.

Interaction of bacterial and archaeal stalk complexes from mesophiles and (hyper)thermophiles with their specific 23S rRNA target sites

The affinity for RNA of isolated L10 is much lower than that of the L10–L12 complex, as reported for EcoL10/$L12_4$ (46,55) and MvaL10/$L12_4$ (26). We could demonstrate the same difference in affinity for L10 and L10/$L12_4$ from the hyperthermophilic *M.jannaschii*. MjaL10 binds the rRNA target site with a rather low affinity (K_d of 2.9×10^{-8} M); in complex with MjaL12, MjaL10 has more than 10-fold

higher affinity (Table 3). Therefore, all experiments were performed with L10–L12 protein complexes.

In the first set of filter-binding experiments, the affinities of the stalk complexes listed in Table 3 for Mja23S-95 and for their homologous 23S rRNA target sites were measured at 37°C in TMK-Cl_{350} buffer, which is very similar to the ribosome reconstitution buffer. Typical binding curves are presented in Figure 8A and B and the K_d values characterizing the interaction of L10–L12 complexes with their 23S rRNA target sites are summarized in Table 3. The saturation level, defined as the percentage of total RNA in complex with protein bound to the nitrocellulose membrane was usually 75 ± 10%. To examine the level of non-specific binding of the stalk complexes, a 120 nt 23S rRNA fragment containing the L1-binding site (49) was used as a negative control. No interaction of any of the stalk complexes with the non-cognate RNA was observed. The affinity of MvaL10/$L12_4$ to the specific 23S rRNA-binding site was low (K_d of $2.4 \pm 0.7 \times 10^{-7}$ M), MthL10/$L12_4$ bound the RNA fragment with a considerably higher affinity (K_d of $5.2 \pm 1.2 \times 10^{-9}$ M), and MjaL10/$L12_4$ and MigL10/$L12_4$ as well as SsoL 10/$L12_4$ exhibited a much higher affinity for Mja23S rRNA (K_d of $6.1 \pm 2.2 \times 10^{-10}$ M; K_d of $8.4 \pm 1.4 \times 10^{-10}$ M; K_d of $1.6 \pm 0.3 \times 10^{-9}$ M, respectively). A similar wide range of dissociation constants was observed for the bacterial complexes. EcoL10/$L12_4$ bound the 23S rRNA fragment with a K_d of $4.1 \pm 1.6 \times 10^{-7}$ M; GstL10/$L12_4$ and TthL10/$L12_6$ displayed K_d values of $5.6 \pm 1.5 \times 10^{-10}$ M and of $2.3 \pm 0.2 \times 10^{-11}$ M, respectively. Thus, the K_d values characterizing the L10/$L12_4$–23S rRNA, and L10/$L12_6$–23S rRNA complexes vary by more than four orders of magnitude. In general, the affinities of the archaeal stalk complexes to their homologous RNA fragments were slightly lower, whereas those of the bacterial stalk complexes to their homologous RNAs was slightly higher (Table 3). To examine the level of non-specific binding of the stalk complexes, a 120 nt 23S rRNA fragment containing the L1-binding site (49) was used as a negative control. No interaction of any of the stalk complexes with the non-cognate RNA was observed. Thus, the K_d values characterizing the L10/$L12_4$–23S rRNA, and L10/$L12_6$–23S rRNA complexes vary by more than four orders of magnitude. A striking correlation between the thermal stability of the stalk complexes (as determined by the heat step in the purification procedure) and the K_d values characterizing their interaction with the 23S rRNA target site was discovered (Figure 9).

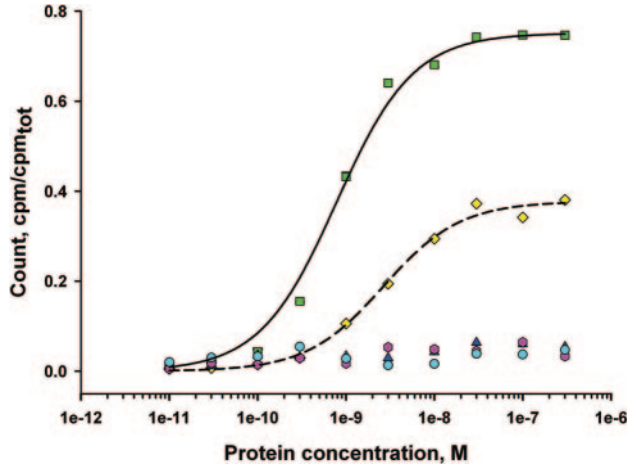

Figure 7. Binding curves for the interaction of L10/$L12_4$ from *M.jannaschii* with different variants of the specific 23S rRNA-binding site. The following designations are used (according to Table 2): MvL10.23S (red); Mja23S-95 (green); Mja23S-80 (yellow); Mja23S-70 (pink); Mja23S-81 (cyan); Mja23S-56 (blue). The fit theoretical curves are plotted for the Mja23S-95 fragment (continuous) and for Mja23S-80 (dashed).

To examine the role of electrostatic interactions in the formation of the L10/$L12_4$–23S rRNA complexes, we determined K_d values of the interaction of the L10/$L12_4$ complexes of the four *Methanococcus* species with Mja23S-95 rRNA in the presence of different concentrations of KCl in the range of 50–800 mM. Binding of the two hyperthermophilic complexes MjaL10/$L12_4$ and MigL10/$L12_4$ was almost insensitive to the KCl concentration. The MthL10/$L12_4$ and MvaL10/$L12_4$ complexes showed only a slight dependence on KCl concentration: the difference in affinity between 50 and 800 mM KCl was less than 0.5log (Figure 10A and B). Therefore, it appears that only few, if any, electrostatic interactions play a role in stabilizing the archaeal L10/$L12_4$–23S rRNA complexes.

TMK_{350} buffers, adjusted to pH values of 6.5, 7.5 and 8.5, were used in filter-binding experiments to test the potential

Table 3. Dissociation constants (K_d's) of stalk complex–23S rRNA complexes and optimal growth temperatures of the source organisms

Protein–RNA complex	K_d ($\times 10^{-8}$ M) in TMK_{350}	Optimal growth temperature of the source organism
MigL10/$L12_4$–Mja23S rRNA	0.084	88°C (*M.igneus*)
MjaL10/$L12_4$–Mja23S rRNA	0.061	
MjaL11–Mja23S rRNA	2.2	85°C (*M.jannaschii*)
MjaL10–Mja23S rRNA	2.9	
MthL10/$L12_4$–Mja23S rRNA	0.52	65°C (*M.thermolithotrophicus*)
MthL10/$L12_4$-Mth23S rRNA	0.87	
MvaL10/$L12_4$–Mja23S rRNA	24	37°C (*M.vannielii*)
SsoL10/$L12_4$–Mja23S rRNA	0.16	75°C (*S.solfataricus*)
SsoL10/$L12_4$-Sso23S rRNA	0.47	
TthL10/$L12_6$–Mja23S rRNA	0.0073	75°C (*T.thermophilus*)
TthL10/$L12_6$–Tth23S rRNA	0.0023	
GstL10/$L12_4$–Mja23S rRNA	0.56	65°C (*G.stearothermophilus*)
GstL10/$L12_4$–Gst23S rRNA	0.16	
EcoL10/$L12_4$–Mja23S rRNA	80	37°C (*E.coli*)
EcoL10/$L12_4$–Eco23S rRNA	41	

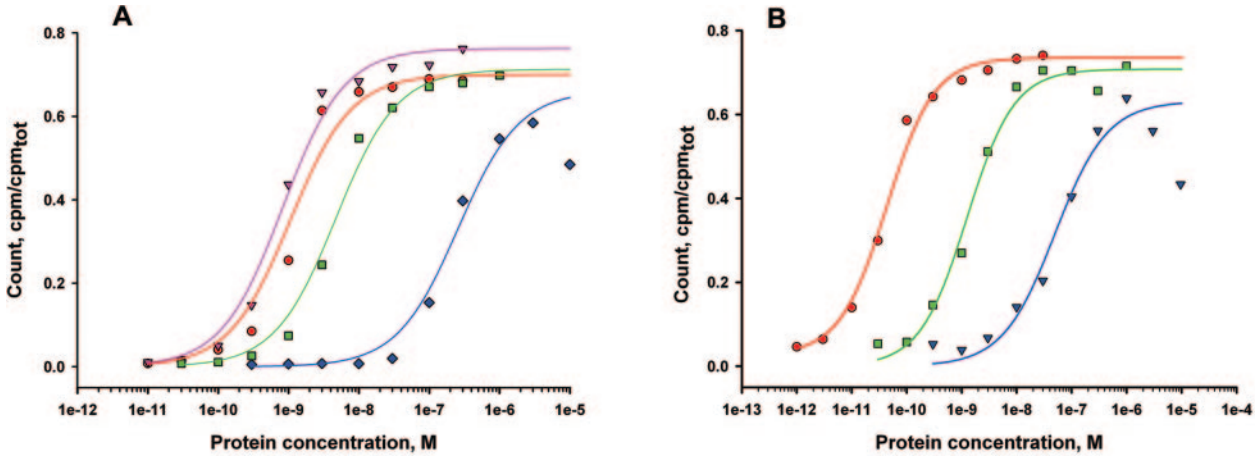

Figure 8. Typical binding curves for the interaction of archaeal (**A**) and bacterial (**B**) stalk complexes with specific 23S rRNA fragments. (A): binding of L10/L12$_4$ from *M.igneus* (red), *M.jannaschii* (pink), *M.thermolithotrophicus* (green) and *M.vannielii* (blue) to the Mja23S-95 rRNA fragment; (B): binding of L10/L12$_6$ from *T.thermophilus* (red), L10/L12$_4$ from *G.stearothermophilus* (green) and *E.coli* (blue) to specific 23S rRNA fragments from the same organisms. The fit theoretical curves are marked with corresponding colors.

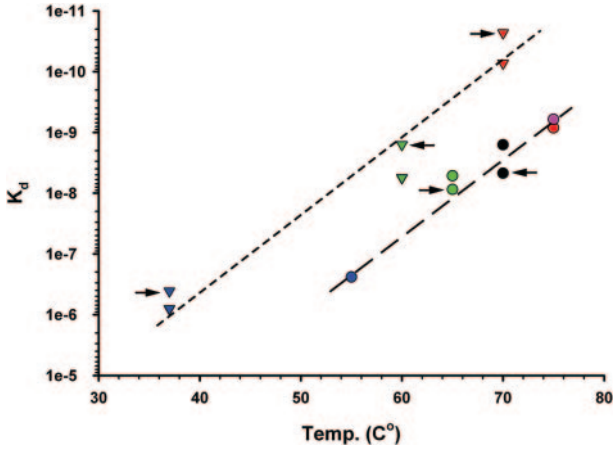

Figure 9. The correlation between K_d values characterizing the interaction of bacterial and archaeal L10–L12 complexes with their 23S rRNA target sites summarized in Table 3 and thermostability of stalk complexes. Triangles: bacterial complexes from *T.thermophilus* (red), *G.stearothermophilus* (green) and *E.coli* (blue). Circles: archaeal complexes from *M.igneus* (red), *M.jannaschii* (pink), *S.solfataricus* (black), *M.thermolithotrophicus* (green) and *M.vannielii* (blue). Points reflecting interaction of the stalk complexes with homologous RNA fragments are marked with arrows.

influence of pH on the affinity for Mja23S-95 of the L10/L12$_4$ complexes of the four *Methanococcus* species. The K_d values were identical at the three different pH values, thus no pH dependence (in the range between 6.5 and 8.5) was observed, no titrable groups influenced complex formation. (data not shown).

To investigate the temperature dependence of L10/L12$_4$–23S rRNA complex formation, the four complexes (MjaL10/L12$_4$, MigL10/L12$_4$, MthL10/L12$_4$ and MvaL10/L12$_4$) were used to test their affinity for Mja23S-95 at temperatures in the range of 0–60°C. To our surprise, the stalk complex MvaL10/L12$_4$ from a mesophilic organism was not only thermostable, but also able to bind the specific RNA target site at 60°C. As an example, typical binding curves for MthL10/L12$_4$ are shown in Figure 11A. The temperature dependence of K_d's for interaction of stalk complexes with the specific rRNA fragment as an Arrhenius plot (logarithms of the K_d's as a function of 1/T) is shown in Figure 11B (56). Binding of MthL10/L12$_4$ to RNA was relatively insensitive to temperature, MvaL10/L12$_4$ binds more effectively at lower temperatures (negative correlation between temperature and affinity), and MigL10/L12$_4$ and MjaL10/L12$_4$ show a higher affinity at higher temperatures (positive correlation between temperature and affinity).

Cooperative effect of binding of r-proteins L10, L11 and L12 with 23S rRNA

A potential cooperative effect of the binding of L10/L12$_4$ and L11 to the 23S rRNA was studied using gel-shift experiments with two color fluorescent staining of the RNA and protein components (40). To assess the role of L11 binding to the specific RNA target site (Figure 6B) for the MvaL10-L12–23S rRNA complex formation, a MjaL11–Mja23S-95 complex was formed in excess of the RNA fragment to give a molar ratio of 1:1 (L11-23S rRNA:free 23S rRNA; Figure 12, lane 2). MvaL10/L12$_4$ bound the rRNA fragment very poorly. Only 14% of the 'active' stalk complex was in complex with rRNA (Figure 12, lane 5). 29% of the MvaL10/L12$_4$ complex forms dimers or multimeric aggregates (top bands in Figure 12, lanes 4 and 5), which do not bind RNA and which therefore are defined as 'inactive'. In the presence of MjaL11, 63% of the active MvaL10/L12$_4$ bound the specific RNA target site (Figure 12, lane 6), which represents a 4.5-fold stimulation of MvaL10/L12$_4$ binding by MjaL11. An identical stimulation was observed when MjaL11 and MvaL10/L12$_4$ were added simultaneously.

A similar approach was used to examine potential stimulation of the binding of L11 to its rRNA target site in the presence of L10/L12$_4$. First, a MjaL10/L12$_4$–Mja23S-95 complex was formed in excess of the RNA fragment to give a molar ratio of 1:1 (L10/L12$_4$-23S rRNA:free 23S

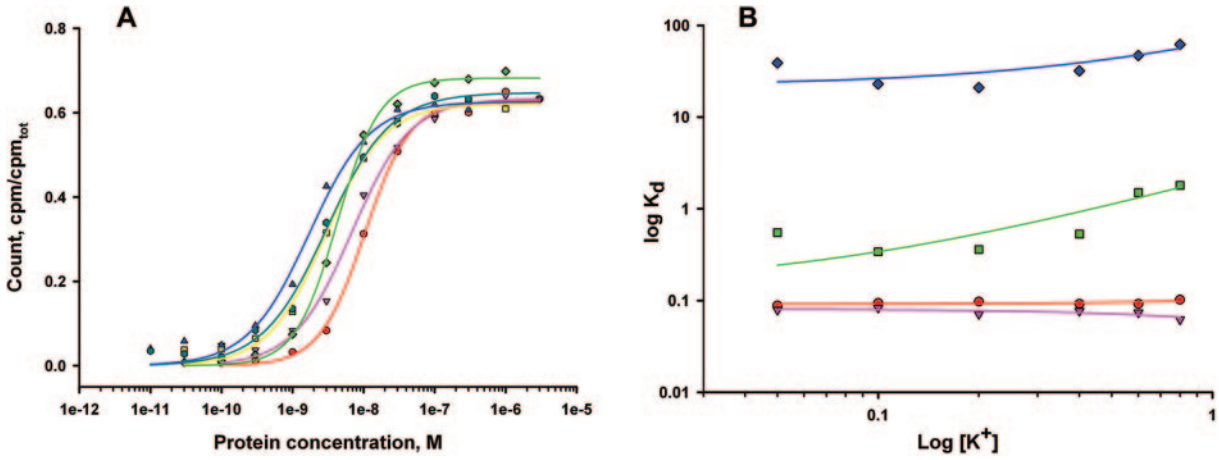

Figure 10. Ionic strength dependence of RNA-binding of archaeal complexes L10/L12$_4$. (**A**) Typical binding curves for the interaction of L10/L12$_4$ from *M.thermolithotrophicus* with the Mja23S-95 rRNA fragment in the presence of different concentrations KCl. 800 mM (red), 600 mM (pink), 400 mM (green), 200 mM (yellow), 100 mM (blue), 50 mM (cyan). The fit theoretical curves are marked with corresponding colors. (**B**) K_d's for the interaction of L10/L12$_4$ from *M.igneus* (red), *M.jannaschii* (pink), *M.thermolithotrophicus* (green) and *M.vannielii* (blue) with the specific Mja23S rRNA fragment were determined with the same KCl concentrations (50–800 mM) and shown as a log–log plot. The best fit theoretical lines are marked with corresponding colors.

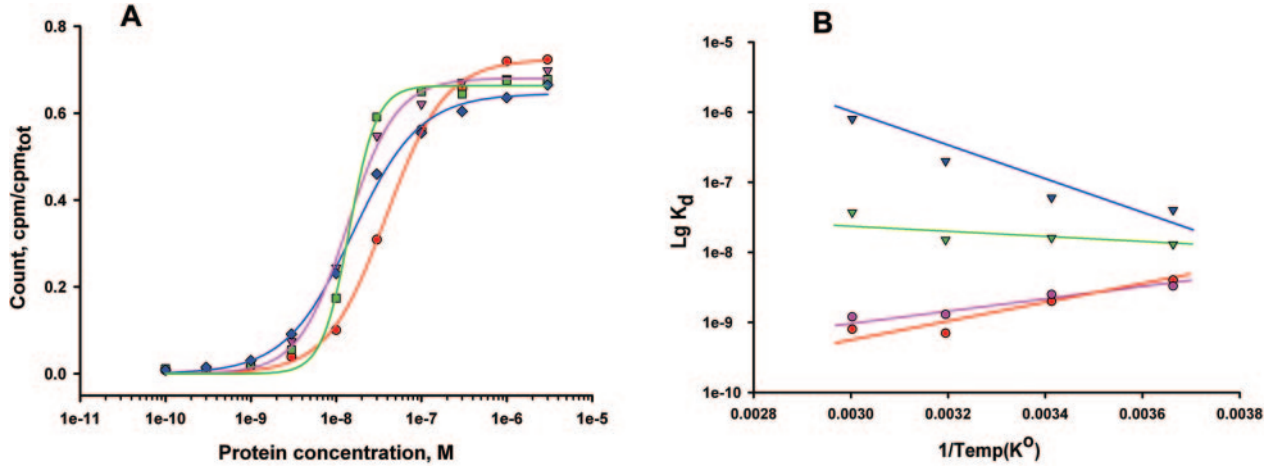

Figure 11. Temperature dependence of RNA-binding of archaeal complexes L10/L12$_4$. (**A**) Typical binding curves for the interaction of L10/L12$_4$ from *M.thermolithotrophicus* with the Mja23S-95 rRNA fragment at 60°C (red), 40°C (pink), 20°C (green) and 0°C (blue). The fit theoretical curves are marked with the corresponding colors. (**B**) Dependence of K_d's for the interaction of L10–L12$_4$ complexes from *M.igneus* (red), *M.jannaschii* (pink), *M.thermolithotrophicus* (green) and *M.vannielii* (blue) with the specific Mja23S-95 rRNA fragment at the same temperatures (0–60°C) shown as an Arrhenius plot (lg K_d's as a function of 1/T). The best fit theoretical lines are marked with the corresponding colors.

rRNA) under standard conditions (37°C; Figure 13, lane 7) and at 70°C (Figure 13, lane 8), then MjaL11 was added. Surprisingly, the binding of MjaL11 to its specific RNA target site was only influenced by the presence of MigL10/L12$_4$ at high temperatures. At 37°C, 56% of MjaL11 was bound to free rRNA and only 44% of MjaL11 was complexed with the rRNA–MigL10/L12$_4$ complex (Figure 13, lane 5). When the binding experiment was performed at 70°C under the same conditions, MjaL11 preferentially bound the 23S rRNA–MigL10/L12$_4$ complex: 87% of MjaL11 was bound to 23S rRNA complexed with L10/L12$_4$, whereas only 13% of MjaL11 was bound to free 23S rRNA (Figure 13, lane 6). Under the given experimental conditions, the affinity of isolated MjaL11 for the specific RNA target site was not influenced by temperature (Figure 13, lanes 2 and 3).

DISCUSSION

Expression and characterization of the L10–L12 complexes

All recombinant L10–L12 complexes used in this study, except that from *M.jannaschii*, were formed in the *E.coli* host cells in a stoichiometry L10:L12 close to 1:4 and 1:6 (*T.thermophilus*), respectively. The same pentameric and heptameric structures were formed as described for complexes isolated from ribosomes of *E.coli* (57), *S.solfataricus* (58) and *T.thermophilus* (21). Thus, it is a reasonable assumption that all recombinant L10/L12$_4$ complexes formed in *E.coli* have the same stoichiometry as the complexes forming the L12 stalk in the ribosome. The long-range coupling of the translation of the L10 and L12 cistrons described for *E.coli* (59) and *M.vannielii* (26,60), which results in the expression

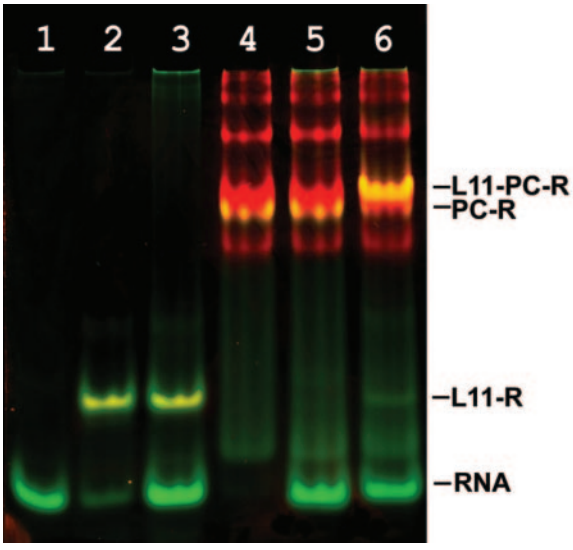

Figure 12. Stimulation of the L10/L12$_4$–RNA interaction in the presence of L11 analyzed by non-denaturing PAGE with two color fluorescent staining. The protein component is visualized with SYPRO® Red Protein Gel Stain (red) and the RNA component with SYBR® Green I (green). The yellow color represents the protein–RNA complexes because of the superimposed green and red signals from the RNA (SYBR Green I) and protein (SYPRO Red) channel. Lane 1, RNA fragment Mja23S-95; lanes 2, 3, MjaL11 mixed with RNA fragment in a molar ratio of 1:1, 1:2 respectively; lanes 4 and 5, MvaL10/L12$_4$ mixed with RNA fragment in a molar ratio of 4:1, 2:1, respectively; lane 6, MvaL10/L12$_4$ mixed with RNA fragment and L11 r-protein in a molar ratio of 2:1:1. RNA, RNA fragment Mja23S-95; PC-R, L10/L12$_4$ bound to RNA; L11-R, L11 bound to RNA; L11-PC-R, complex of L11 and L10/L12$_4$ with RNA.

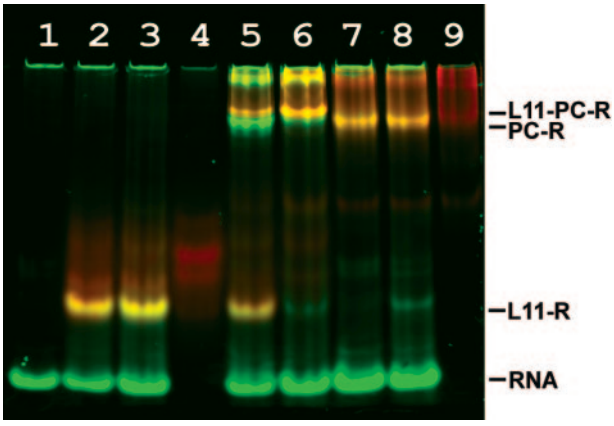

Figure 13. Stimulation of the L11–RNA interaction by L10/L12$_4$, analyzed by non-denaturing PAGE with two color fluorescent staining. The protein component was pre-labeled (i.e. before complex formation) with TAMRA (red) and the gel was stained with SYBR® Green I, specific for RNA (green). The yellow color represents the protein–RNA complexes because of the superimposed green and red signals from the RNA (SYBR Green I) and protein (TAMRA) channel. Lane 1, RNA fragment Mja23S-95; lanes2 and 3, pre-labeled MjaL11 mixed with the RNA fragment in a molar molar ratio of 1:2, incubated at 37 and 70°C, respectively; 4, pre-labeled MjaL11; lanes 5 and 6, mixture of MigL10/L12$_4$–RNA–pre-labeled MjaL11 in a molar ratio of 1:2:1, incubated at 37 and 70°C, respectively; lanes 7 and 8, pre-labeled MigL10/L12$_4$ mixed with RNA fragment in a molar ratio of 1:2, incubated at 37 and 70°C, respectively; 9, pre-labeled MigL10/L12$_4$. RNA, RNA fragment Mja23S-95; PC-R, L10/L12$_4$ bound to RNA; L11-R, L11 bound to RNA; L11-PC-R, complex of L11 and L10/L12$_4$ with RNA.

of L10 and L12 in a ratio of 1:4, (1:6 for *T.thermophilus*), functions in the *E.coli* host. The translational coupling mechanism ensures the co-ordinate expression of genes, which are encoded on one mRNA. According to this model, the L12 gene is not efficiently expressed from its own Shine–Dalgarno sequence unless the preceding L10 gene is also expressed.

The L12 proteins from (hyper)thermophilic *Methanococcus* species (*M.igneus*, *M.jannaschii*, *M.thermolithotrophicus*), which are closely related (66–83% of identity of amino acid sequence) showed an 'anomalous' mobility in SDS–PAGE which was not in accordance with their MWs, even after increasing the denaturing effect of SDS by adding 8M to the gel and formamide to the loading buffer (Figures 4 and 5). These recombinant L12 proteins were of the correct size and had no post-translational modifications, as shown by mass-spectrometry. A possible explanation for the 'abnormal' mobility of MigL12 and MjaL12 (MWs close to 20 000) is that their dimeric structure could not be dissolved. They still form dimers, even under very harsh denaturing condition, Di-, tri- and tetrameric forms in solution were earlier observed for L12 from the thermophilic Bacterium *T.maritima* (61).

As for MthL12, which shows a MW of about 15 000, we speculate that the secondary and tertiary structures did not denature completely and prevented equal SDS-binding, decreasing their mobility in SDS–PAGE. This assumption is supported by the fact that the mobility of SsoL12 was according to its calculated MW only under very harsh denaturing conditions (Figure 4 lane10; Figure 5, lane 6). We suggest that described differences in the mobility of the L12 proteins in SDS–PAGE (with or without urea) reflect the dissimilarity of some structural features (e.g. stability of the hydrophobic core or secondary structure elements) in the proteins. It is tempting to speculate that the increasing stability of secondary and/or tertiary structure elements, in the order *M.vannielii* → *M.thermolithotrophicus* → *M.jannaschii* → *M.igneus*, is a high temperature adaptation, optimizing the small proteins for thermal demands (2).

Interaction of archaeal and bacterial stalk complexes with specific 23S rRNA fragments

Based on the early RNAase and chemical probing data of 23S rRNA (51,52), in combination with the structure of the L11–rRNA complex (53,54) and of the structure of the TthL10$_{NTD}$–23S rRNA complex (22) it was obvious that helix 42 (Figure 6A and B) plays a major role in L10–23S rRNA interaction. Phylogenetic sequence alignments of the nucleotide sequences of L10 binding sites on the 23S (28S) rRNAs revealed very high level of homology among Bacteria, Archaea and Eukarya. Comparison of the putative secondary structures of these sites demonstrated even more similarity (51). We tried to minimize the L10 binding site of 23S rRNA by deleting helixes 43a, 43 and 44 (Figure 6B) of the thiostrepton loop. Only one part—helix 43a—could be eliminated without completely losing binding capacity; but the saturation level was drastically reduced (Figure 7). This observed great decrease of saturation with only a small influence on affinity could be a result of rRNA misfolding.

L10 interacts predominantly with the sugar-phosphate backbone of a number of discontinuous regions of the rRNA and therefore seems to recognize the overall structure of the L10/L11 binding region of 23S rRNA, and in particular, the upper stem of helix 42 and the loops connecting helixes 42–43 and 43–44 (22). L10 probably only contacts helix 42 and the upper loop directly. Thus, even if most of the thiostrepton loop was not directly involved in L10 binding (probably this is correct at least for helix 43a), this 23S rRNA region seems to participate in forming the correct conformation of the binding site. Our results indicate that all the other elements of this 23S rRNA area (Figure 6A and B) are required for proper folding of the L10 binding site.

Despite the lack of significant overall sequence identity between bacterial and archaeal L10 NTDs, the secondary structure elements of the $TmaL10_{NTD}$ seem to be very similar to the $HmaL10_{NTD}$. Therefore, bacterial and archaeal L10 probably bind to 23S rRNA in a similar manner.

The determined apparent K_d's (Table 3) show that all protein complexes effectively interacted with all RNA fragments. The source of RNA fragment has little effect on the affinity. Only minor systematic differences were observed between archaeal and bacterial RNA fragments: in general bacterial stalk complexes showed slightly higher affinity to homologous (bacterial) RNA fragments than to archaeal ones (Table 3 and Figure 9). The drastic differences in affinity between 23S rRNA and stalk complexes from meso-, thermo- and hyperthermophilic microorganisms are determined by the protein partner as was previously demonstrated for r-proteins L1 (49), S4 (15) and S8 (14). The K_d's determined in buffer with an average KCl concentration (350 mM) for hyperthermophilic $MigL10/L12_4$–RNA and $MjaL10/L12_4$–RNA complexes were about one order of magnitude higher than that for thermophilic $MthL10/L12_4$–RNA and more than two orders of magnitude higher than that for mesophilic $MvaL10/L12_4$–RNA (Table 3). The bacterial heptameric complex $TthL10/L12_6$ has an extremely high affinity (the highest ever determined among all ribosomal proteins) both to the archaeal and its own specific 23S rRNA fragments, about one order of magnitude higher than the pentameric complexes from the hyperthermophilic *M.igneus* and *M.jannaschii*, in spite of the fact that the optimal growth temperature of *T.thermophilus* is lower. We cannot exclude that this extraordinary high affinity (i.e. stability of the RNA–protein complex) is due to the presence of one additional dimer of L12. Of course, this effect must be indirect, as the the crystal structure of the TthL10IL12 complex and previous studies on the lack of interaction of L12 with RNA exclude a direct interaction of the third dimmer with RNA.

Thus our binding data confirmed the assumption that stronger protein–RNA interactions are typical for (hyper) thermophilic species and probably make a substantial contribution to the thermal stability of r-protein–rRNA complexes (and the ribosome as a whole). The lower affinity of r-proteins from thermophilic species and the much lower affinity of r-proteins from mesophilic species might result in a gain of flexibility by the ribosome. Higher flexibility might be a prerequisite for full activity of the ribosome at lower temperatures. Therefore, the stability of the individual rRNA–protein complexes within the ribosome modulates the stability of the ribosome and provides an optimum thermostability/flexibility balance at the growth temperature of the organism.

The salt dependence of $L10/L12_4$–rRNA-binding for all four archaeal $L10/L12_4$ complexes was very weak over the range of 50 to 800 mM KCl. (Figure 10A and B). In general, it appeared that only few, if any, electrostatic interactions play a role in stabilizing the $L10/L12_4$–23S rRNA complex. This conclusion is in agreement with the model of 23S rRNA–$HmaL10_{NTD}$ interaction (22), where hydrogen bonds and hydrophobic interactions make a major contribution to RNA–protein binding. In the cases of the $MthL10/L12_4$ and $MvaL10/L12_4$ complexes (Figure 10B), the ionic contacts contribute a bit more to the interaction, possibly because of increased conformational flexibility of those complexes.

Ionic strength dependence of r-protein–RNA interactions is variable, from very weak for r-protein S4 (62) to intermediate for L11 (63). Measurement of the salt dependence of protein–RNA-binding with subsequent structural study cautions against using the salt dependence of specific protein–RNA complexes alone to count ionic interactions and shows that the interactions of many basic residues have been misidentified, as shown in the case of the well studied L11–rRNA complex (58). Though salt dependence data are difficult to interpret quantitatively, it is useful to appreciate the electrostatic contribution in RNA–protein complex formation [reviewed in (64)].

The temperature dependence of binding of different pentameric complexes to rRNA is presented in Figure 11. Whereas $MthL10/L12_4$ (from a thermophilic organism) binding was almost insensitive to temperature, $MvaL10/L12_4$ (from a mesophilic organism) required lower temperatures for more effective binding (negative correlation between temperature and K_d), while $MigL10/L12_4$ and $MjaL10/L12_4$ (from hyperthermophilic organisms) demonstrated an opposite effect (positive correlation between temperature and K_d). We suppose that this correlation is elucidated by the interference of two different effects. First, the $L10/L12_4$ complexes might undergo reversible, temperature-dependent conformational changes that can be favorable (especially for extremely thermostable r-proteins with rigid structure) or excessive and unfavorable (for non-thermostable r-proteins with flexible structure). Second, the thermal dissociation might make a negative contribution (especially for low affinity binding r-proteins from mesophiles). The weak temperature dependence of $MthL10/L12_4$ binding capacity could be a result of mutual compensation of both factors whereas in other cases ($MvaL10/L12_4$, $MigL10/L12_4$ or $MjaL10/L12_4$) one of the factors probably predominates. This characteristic feature of the $MthL10/12_4$ complex correlates with the unusual wide range of temperature at which *M.thermolithotrophicus* can grow (65), in contrast to other *Methanococcus* species.

Cooperative effect of binding of r-proteins L10, L11 and L12 to the specific RNA fragment

Early studies demonstrated that r-protein L10 in the absence of L12 interacts with 23S rRNA very weakly, whereas the isolated r-protein L12 does not interact with rRNA (46,55). L12 does not bind directly to the 23S rRNA, but only via the r-protein L10 (66)), for review see (67). It was also

shown that the presence of L12 greatly enhanced the affinity of L10 for 23S rRNA. However there are very few studies about interaction of the isolated r-protein L10 with rRNA, partly because of the instability of this r-protein in solution (68).

In our work we demonstrated that stimulation of L10 affinity by L12 takes place also in thermophilic organisms [as it was shown for the mesophilic *E.coli* (46,55) and *M.vannielii* (26)]. In contrast to L10 from *E.coli*, L10 from the hyperthermophilic Archaeon *M.jannaschii* is quite stable in solution and despite a tendency to aggregate in the isolated state (data not shown), MjaL10 has a rather high affinity for the specific 23S rRNA fragment (K_d of 2.9×10^{-8} M). Addition of r-protein MjaL12 drastically increases binding capacity of MjaL10 (50-fold, up to K_d of $6.1 - 7.1 \times 10^{-10}$ M). The mechanism of this phenomenon is probably related to conformational changes of L10 during its interaction with L12, but our limited knowledge about the 3D structure of L10 in different states (free; L12 bound; 23S rRNA bound) precludes the proposal of a model of this process. The analysis of the bacterial TmaL10/$(L12_{NTD})_6$ structure demonstrated only rather weak interactions (one salt bridge) between the proximal $L12_{NTD}$ molecule and RNA-bound $L10_{NTD}$ (22).

Binding of L11 and the stalk complex to 23S rRNA has been studied in detail because both of them participate in the formation of the GTPase binding site on the ribosome. Early investigations demonstrated, in particular, that the binding of L10/$L12_4$ to 23S rRNA in *E.coli* is stimulated by L11 and vice versa (46). Later, interactions of the individual L11 protein and the L10/$L12_4$ complex with 23S rRNA in *E.coli* were studied in more detail (51,52) Cooperative effects of binding L11 and L10/$L12_4$ to 23S rRNA have been corroborated by experiments on interaction of these proteins with mutant 23S rRNAs (69). In view of the differences between archaeal and bacterial stalk complexes, (see Introduction) we investigated a cooperative effect of MjaL11 and the complexes MjaL10/$L12_4$ and MvaL10/$L12_4$ in binding to the specific 23S rRNA fragment Mja23S-95. We observed stimulation of binding of the L10–$L12_4$ complex by the r-protein L11 and stimulation of binding of the r-protein L11 by the L10/$L12_4$ complex (Figures 12 and 13). Interestingly, stimulation of the L11–rRNA interaction by MjaL10/$L12_4$ occurred only at high temperature (70°C) whereas at 37°C no stimulation was observed.

The most probable reason for such cooperativity in L11–L10/$L12_4$–23S rRNA interaction is the conformational ordering of the rRNA during binding of one of these proteins, which facilitates the interaction of the other partner with the rRNA. On the other hand, the influence of direct interaction between L11 and L10, as proposed in a recent model (22), during their binding to 23S rRNA also cannot be excluded.

ACKNOWLEDGEMENTS

The authors thank Prof. S. Nikonov, Dr N. Nevskaya and Dr V. Filimonov (IPR, RAS, Pushchino, Russia) for very helpful discussions and M. Humpel for excellent technical assistance. The genomic DNA from *G.stearothermophilus* was kindly provided by N. Matvienko (IPR, RAS, Pushchino, Russia). The authors are much obliged to Peter Kaiser for critical reading of the manuscript. This work was supported by the Austrian Science Fund (FWF) grant P-17164-B10 to W.P. The research of M.G. was supported the Russian Academy of Sciences, the Russian Foundation for Basic Research, the Program of RAS on Molecular and Cellular Biology and the Program of the RF President on support of outstanding scientific schools RI-112/001/391 and in part by an International Research Scholar's award from the Howard Hughes Medical Institute. Funding to pay the Open Access publication charges for this article was provided by the Austrian Science Fund (FWF).

Conflict of interest statement. None declared.

REFERENCES

1. Haney,P.J., Badger,J.H., Buldak,G.L., Reich,C.I., Woese,C.R. and Olsen,G.J. (1999) Thermal adaptation analyzed by comparison of protein sequences from mesophilic and extremely thermophilic *Methanococcus* species. *Proc. Natl Acad. Sci. USA*, **96**, 3578–3583.
2. Jaenicke,R. and Bohm,G. (1998) The stability of proteins in extreme environments. *Curr. Opin. Struct. Biol.*, **8**, 738–748.
3. Karshikoff,A. and Ladenstein,R. (2001) Ion pairs and the thermotolerance of proteins from hyperthermophiles: a 'traffic rule' for hot roads. *Trends Biochem. Sci.*, **26**, 550–556.
4. Yusupov,M.M., Yusupova,G.Z., Baucom,A., Lieberman,K., Earnest,T.N., Cate,J.H. and Noller,H.F. (2001) Crystal structure of the ribosome at 5.5 A resolution. *Science*, **292**, 883–896.
5. Pedone,F., Bonincontro,A., Briganti,G., Giansanti,A., Londei,P., Risuleo,G. and Mengoni,M. (1997) Effects of magnesium and temperature on the conformation and reassociation of *Escherichia coli* and *Sulfolobus solfataricus* ribosomes. *Biochim. Biophys. Acta*, **1335**, 283–289.
6. Cammarano,P., Mazzei,F., Londei,P., Teichner,A., de Rosa,M. and Gambacorta,A. (1983) Secondary structure features of ribosomal RNA species within intact ribosomal subunits and efficiency of RNA-protein interactions in thermoacidophilic (*Caldariella acidophila, Bacillus acidocaldarius*) and mesophilic (*Escherichia coli*) bacteria. *Biochim. Biophys. Acta*, **740**, 300–312.
7. Altamura,S., Caprini,E., Sanchez,M.E. and Londei,P. (1991) Early assembly proteins of the large ribosomal subunit of the thermophilic archaebacterium *Sulfolobus*. Identification and binding to heterologous rRNA species. *J. Biol. Chem.*, **266**, 6195–6200.
8. Briganti,G., Giordano,R., Londei,P. and Pedone,F. (1998) Small angle neutron scattering analysis of thermal stability of 23S rRNA and the intact 50S subunits of *Sulfolobus solfataricus*. *Biochim. Biophys. Acta*, **1379**, 297–301.
9. Wang,H.C. and Hickey,D.A. (2002) Evidence for strong selective constraint acting on the nucleotide composition of 16S ribosomal RNA genes. *Nucleic Acids Res.*, **30**, 2501–2507.
10. Galtier,N. and Lobry,J.R. (1997) Relationships between genomic G+C content, RNA secondary structures, and optimal growth temperature in prokaryotes. *J. Mol. Evol.*, **44**, 632–636.
11. Noon,K.R., Bruenger,E. and McCloskey,J.A. (1998) Posttranscriptional modifications in 16S and 23S rRNAs of the archaeal hyperthermophile *Sulfolobus solfataricus*. *J. Bacteriol.*, **180**, 2883–2888.
12. McCloskey,J.A., Graham,D.E., Zhou,S., Crain,P.F., Ibba,M., Konisky,J., Söll,D. and Olsen,G.J. (2001) Post-transcriptional modification in archaeal tRNAs: identities and phylogenetic relations of nucleotides from mesophilic and hyperthermophilic *Methanococcales*. *Nucleic Acids Res.*, **29**, 4699–4706.
13. Kraft,A., Lutz,C., Lingenhel,A., Gröbner,P. and Piendl,W. (1999) Control of ribosomal protein L1 synthesis in mesophilic and thermophilic archaea. *Genetics*, **152**, 1363–1372.
14. Gruber,T., Köhrer,C., Lung,B., Shcherbakov,D. and Piendl,W. (2003) Affinity of ribosomal protein S8 from mesophilic and (hyper)thermophilic archaea and bacteria for 16S rRNA correlates with the growth temperatures of the organisms. *FEBS Lett.*, **549**, 123–128.
15. Gerstner,R.B., Pak,Y. and Draper,D.E. (2001) Recognition of 16S rRNA by ribosomal protein S4 from *Bacillus stearothermophilus*. *Biochemistry*, **40**, 7165–7173.

16. Rassokhin,T.I., Golovin,A.V., Petrova,E.B., Spiridonova,V.A., Karginova,O.A., Rozhdestvenskii,T.S., Brosius,J. and Kopylov,A.M. (2001) [Study of the binding of the S7 protein with 16S rRNA fragment 926-986/1219-1393 as a key step in the assembly of the small subunit of prokaryotic ribosomes]. *Mol. Biol. (Mosk)*, **35**, 617–627.
17. Wimberly,B.T., Brodersen,D.E., Clemons,W.M., Jr, Morgan-Warren,R.J., Carter,A.P., Vonrhein,C., Hartsch,T. and Ramakrishnan,V. (2000) Structure of the 30S ribosomal subunit. *Nature*, **407**, 327–339.
18. Brodersen,D.E., Clemons,W.M., Jr, Carter,A.P., Wimberly,B.T. and Ramakrishnan,V. (2002) Crystal structure of the 30 S ribosomal subunit from *Thermus thermophilus*: structure of the proteins and their interactions with 16S RNA. *J. Mol. Biol.*, **316**, 725–768.
19. Burggraf,S., Fricke,H., Neuner,A., Kristjansson,J., Rouvier,P., Mandelco,L., Woese,C.R. and Stetter,K.O. (1990) *Methanococcus igneus sp. nov.,* a novel hyperthermophilic methanogen from a shallow submarine hydrothermal system. *Syst. Appl. Microbiol.*, **13**, 263–269.
20. Criswell,A.R., Bae,E., Stec,B., Konisky,J. and Phillips,G.N., Jr (2003) Structures of thermophilic and mesophilic adenylate kinases from the genus *Methanococcus*. *J. Mol. Biol.*, **330**, 1087–1099.
21. Ilag,L.L., Videler,H., McKay,A.R., Sobott,F., Fucini,P., Nierhaus,K.H. and Robinson,C.V. (2005) Heptameric $(L12)_6$/L10 rather than canonical pentameric complexes are found by tandem MS of intact ribosomes from thermophilic bacteria. *Proc. Natl Acad. Sci. USA*, **102**, 8192–8197.
22. Diaconu,M., Kothe,U., Schlunzen,F., Fischer,N., Harms,J.M., Tonevitsky,A.G., Stark,H., Rodnina,M.V. and Wahl,M.C. (2005) Structural basis for the function of the ribosomal L7/12 stalk in factor binding and GTPase activation. *Cell*, **121**, 991–1004.
23. Rodnina,M.V. and Wintermeyer,W. (2003) Peptide bond formation on the ribosome: structure and mechanism. *Curr. Opin. Struct. Biol.*, **13**, 334–340.
24. Montesano-Roditis,L., Glitz,D.G., Traut,R.R. and Stewart,P.L. (2001) Cryo-electron microscopic localization of protein L7/L12 within the *Escherichia coli* 70 S ribosome by difference mapping and Nanogold labeling. *J. Biol. Chem.*, **276**, 14117–14123.
25. Johnsen,M., Christensen,T., Dennis,P.P. and Fiil,N.P. (1982) Autogenous control: ribosomal protein L10-L12 complex binds to the leader sequence of its mRNA. *EMBO J.*, **1**, 999–1004.
26. Mayer,C., Köhrer,C., Gröbner,P. and Piendl,W. (1998) MvaL1 autoregulates the synthesis of the three ribosomal proteins encoded on the MvaL1 operon of the archaeon *Methanococcus vannielii* by inhibiting its own translation before or at the formation of the first peptide bond. *Mol. Microbiol.*, **27**, 455–468.
27. Moller,W., Schrier,P.I., Maassen,J.A., Zantema,A., Schop,E., Reinalda,H., Cremers,A.F. and Mellema,J.E. (1983) Ribosomal proteins L7/L12 of *Escherichia coli*. Localization and possible molecular mechanism in translation. *J. Mol. Biol.*, **163**, 553–573.
28. Stark,H., Rodnina,M.V., Rinke-Appel,J., Brimacombe,R., Wintermeyer,W. and van Heel,M. (1997) Visualization of elongation factor Tu on the *Escherichia coli* ribosome. *Nature*, **389**, 403–406.
29. Noller,H.F. (1984) Structure of ribosomal RNA. *Annu. Rev. Biochem.*, **53**, 119–162.
30. Liao,D. and Dennis,P.P. (1994) Molecular phylogenies based on ribosomal protein L11, L1, L10, and L12 sequences. *J. Mol. Evol.*, **38**, 405–419.
31. Nomura,T., Mochizuki,R., Dabbs,E.R., Shimizu,Y., Ueda,T., Hachimori,A. and Uchiumi,T. (2003) A point mutation in ribosomal protein L7/L12 reduces its ability to form a compact dimer structure and to assemble into the GTPase center. *Biochemistry*, **42**, 4691–4698.
32. Ban,N., Nissen,P., Hansen,J., Moore,P.B. and Steitz,T.A. (2000) The complete atomic structure of the large ribosomal subunit at 2.4 A resolution. *Science*, **289**, 905–920.
33. Harms,J., Schluenzen,F., Zarivach,R., Bashan,A., Gat,S., Agmon,I., Bartels,H., Franceschi,F. and Yonath,A. (2001) High resolution structure of the large ribosomal subunit from a mesophilic eubacterium. *Cell*, **107**, 679–688.
34. Bocharov,E.V., Gudkov,A.T. and Arseniev,A.S. (1996) Topology of the secondary structure elements of ribosomal protein L7/L12 from *E.coli* in solution. *FEBS Lett.*, **379**, 291–294.
35. Bocharov,E.V., Gudkov,A.T., Budovskaya,E.V. and Arseniev,A.S. (1998) Conformational independence of N- and C-domains in ribosomal protein L7/L12 and in the complex with protein L10. *FEBS Lett.*, **423**, 347–350.
36. Mulder,F.A., Bouakaz,L., Lundell,A., Venkataramana,M., Liljas,A., Akke,M. and Sanyal,S. (2004) Conformation and dynamics of ribosomal stalk protein L12 in solution and on the ribosome. *Biochemistry*, **43**, 5930–5936.
37. Bocharov,E.V., Sobol,A.G., Pavlov,K.V., Korzhnev,D.M., Jaravine,V.A., Gudkov,A.T. and Arseniev,A.S. (2004) From structure and dynamics of protein L7/L12 to molecular switching in ribosome. *J. Biol. Chem.*, **279**, 17697–17706.
38. Wahl,M.C., Bourenkov,G.P., Bartunik,H.D. and Huber,R. (2000) Flexibility, conformational diversity and two dimerization modes in complexes of ribosomal protein L12. *EMBO J.*, **19**, 174–186.
39. Moens,P.D., Wahl,M.C. and Jameson,D.M. (2005) Oligomeric state and mode of self-association of *Thermotoga maritima* ribosomal stalk protein L12 in solution. *Biochemistry*, **44**, 3298–3305.
40. Shcherbakov and Piendl, *Electrophoresis*, in press.
41. Jarsch,M., Altenbuchner,J. and Bck,A. (1983) Physical organization of the ribosomal RNAs genes in *Methanococcus vannielii*. *Mol. Gen. Genet.*, **189**, 41–47.
42. Dubendorff,J.W. and Studier,F.W. (1991) Creation of a T7 autogene. Cloning and expression of the gene for bacteriophage T7 RNA polymerase under control of its cognate promoter. *J. Mol. Biol.*, **219**, 61–68.
43. Studier,F.W. and Moffatt,B.A. (1986) Use of bacteriophage T7 RNA polymerase to direct selective high-level expression of cloned genes. *J. Mol. Biol.*, **189**, 113–130.
44. Calderone,T.L., Stevens,R.D. and Oas,T.G. (1996) High-level misincorporation of lysine for arginine at AGA codons in a fusion protein expressed in *Escherichia coli*. *J. Mol. Biol.*, **262**, 407–412.
45. Brinkmann,U., Mattes,R.E. and Buckel,P. (1989) High-level expression of recombinant genes in *Escherichia coli* is dependent on the availability of the dnaY gene product. *Gene*, **85**, 109–114.
46. Dijk,J., Garrett,R.A. and Muller,R. (1979) Studies on the binding of the ribosomal protein complex L7/12-L10 and protein L11 to the 5′-one third of 23S RNA: a functional centre of the 50S subunit. *Nucleic Acids Res.*, **6**, 2717–2729.
47. Williams,M., Brys,A., Weiner,A.M. and Maizels,N. (1992) A rapid method for determining the molecular weight of a protein bound to nucleic acid in a mobility shift assay. *Nucleic Acids Res.*, **20**, 4935–4936.
48. Papac,D.I., Schey,K.L. and Knapp,D.R. (1991) Combination electrospray-liquid secondary ion mass spectrometry ion source. *Anal. Chem.*, **63**, 1658–1660.
49. Köhrer,C., Mayer,C., Neumair,O., Gröbner,P. and Piendl,W. (1998) Interaction of ribosomal L1 proteins from mesophilic and thermophilic Archaea and Bacteria with specific L1-binding sites on 23S rRNA and mRNA. *Eur. J. Biochem.*, **256**, 97–105.
50. Griaznova,O. and Traut,R.R. (2000) Deletion of C-terminal residues of *Escherichia coli* ribosomal protein L10 causes the loss of binding of one L7/L12 dimer: ribosomes with one L7/L12 dimer are active. *Biochemistry*, **39**, 4075–4081.
51. Egebjerg,J., Douthwaite,S.R., Liljas,A. and Garrett,R.A. (1990) Characterization of the binding sites of protein L11 and the L10.$(L12)_4$ pentameric complex in the GTPase domain of 23 S ribosomal RNA from *Escherichia coli*. *J. Mol. Biol.*, **213**, 275–288.
52. Rosendahl,G. and Douthwaite,S. (1993) Ribosomal proteins L11 and L10.$(L12)_4$ and the antibiotic thiostrepton interact with overlapping regions of the 23 S rRNA backbone in the ribosomal GTPase centre. *J. Mol. Biol.*, **234**, 1013–1020.
53. Conn,G.L., Draper,D.E., Lattman,E.E. and Gittis,A.G. (1999) Crystal structure of a conserved ribosomal protein-RNA complex. *Science*, **284**, 1171–1174.
54. Wimberly,B.T., Guymon,R., McCutcheon,J.P., White,S.W. and Ramakrishnan,V. (1999) A detailed view of a ribosomal active site: the structure of the L11-RNA complex. *Cell*, **97**, 491–502.
55. Beauclerk,A.A., Cundliffe,E. and Dijk,J. (1984) The binding site for ribosomal protein complex L8 within 23 s ribosomal RNA of *Escherichia coli*. *J. Biol. Chem.*, **259**, 6559–6563.
56. Ryan,P.C. and Draper,D.E. (1989) Thermodynamics of protein-RNA recognition in a highly conserved region of the large-subunit ribosomal RNA. *Biochemistry*, **28**, 9949–9956.
57. Osterberg,R., Sjoberg,B., Pettersson,I., Liljas,A. and Kurland,C.G. (1977) Small-angle X-ray scattering study of the protein complex of

L7/L12 and L10 from *Escherichia coli* ribosomes. *FEBS Lett*., **73**, 22–24.
58. Casiano,C. and Traut,R.R. (1991) Protein topography of *Sulfolobus solfataricus* ribosomes by cross-linking with 2-iminothiolane. Sso L12e, Sso L10e, and Sso L11e are neighbors. *J. Biol. Chem*., **266**, 21578–21583.
59. Petersen,C. (1989) Long-range translational coupling in the rplJL-rpoBC operon of *Escherichia coli*. *J. Mol. Biol*., **206**, 323–332.
60. Hanner,M., Mayer,C., Köhrer,C., Golderer,G., Gröbner,P. and Piendl,W. (1994) Autogenous translational regulation of the ribosomal MvaL1 operon in the archaebacterium *Methanococcus vannielii*. *J. Bacteriol*., **176**, 409–418.
61. Wahl,M.C., Huber,R., Marinkovic,S., Weyher-Stingl,E. and Ehlert,S. (2000) Structural investigations of the highly flexible recombinant ribosomal protein L12 from *Thermotoga maritima*. *Biol. Chem*., **381**, 221–229.
62. Vartikar,J.V. and Draper,D.E. (1989) S4-16 S ribosomal RNA complex. Binding constant measurements and specific recognition of a 460-nucleotide region. *J. Mol. Biol*., **209**, 221–234.
63. GuhaThakurta,D. and Draper,D.E. (2000) Contributions of basic residues to ribosomal protein L11 recognition of RNA. *J. Mol. Biol*., **295**, 569–580.
64. Draper,D.E. (1999) Themes in RNA-protein recognition. *J. Mol. Biol*., **293**, 255–270.
65. Huber,H., Thomm,M., König,H., Thies,G. and Stetter,K.O. (1982) *Methanococcus thermolithotrophicus*, a novel thermophilic lithotrophic methanogen. *Arch. Microbiol*., **132**, 47–50.
66. Spierer,P., Wang,C.C., Marsh,T.L. and Zimmermann,R.A. (1979) Cooperative interactions among protein and RNA components of the 50S ribosomal subunit of *Escherichia coli*. *Nucleic Acids Res*., **6**, 1669–1682.
67. Gonzalo,P. and Reboud,J.P. (2003) The puzzling lateral flexible stalk of the ribosome. *Biol. Cell*, **95**, 179–193.
68. Petersen,C. (1990) *Escherichia coli* ribosomal protein L10 is rapidly degraded when synthesized in excess of ribosomal protein L7/L12. *J. Bacteriol*., **172**, 431–436.
69. Rosendahl,G. and Douthwaite,S. (1995) Cooperative assembly of proteins in the ribosomal GTPase centre demonstrated by their interactions with mutant 23S rRNAs. *Nucleic Acids Res*., **23**, 2396–2403.